

Effect of the Length of the Poloidal Ducts on Flow Balancing in a Liquid Metal Blanket

Tyler J. Rhodes*, Sergey Smolentsev, Mohamed Abdou

UCLA, MAE Department, 44-114 Engineering IV, 420 Westwood Plaza, Los Angeles, CA 90095-1597, USA

To address concerns associated with liquid metal (LM) flow balancing among multiple poloidal channels of a LM blanket, we investigate the factors (first of all the length of the channels) that influence the flow distribution when the duct walls are electrically insulated. We simulate LM MHD flow through multiple channels fed by a prototypical manifold for a range of channel lengths using a 3D MHD solver, HIMAG. The simplified manifold geometry consists of a rectangular, electrically insulated feeding duct which suddenly expands such that the duct thickness in the magnetic field direction abruptly increases by a factor of 4. After a short length downstream of the expansion, the flow is divided into three identical parallel channels. By measuring the flow rate in each of the channels, we conclude that flow balance among the channels is improved by increasing the length of the channels. An effort is made to obtain scaling laws that characterize flow balancing as a function of the flow parameters and the manifold geometry using a Resistor Network Model (RNM). Associated Hartman and Reynolds numbers in the computations were $\sim 10^3$ and 10^2 respectively. Compared to the full 3D analysis, the proposed RNM suggests a relatively quick and simpler way of computing the blanket length that might be needed to provide balanced flow among the parallel channels.

Keywords: Manifold, MHD, Liquid Metal, Flow Balancing, Blanket

1. Introduction

Liquid metal (LM) blankets for power fusion reactors circulate LM (Li or PbLi) in the presence of a strong plasma-confining magnetic field for breeding tritium, transferring heat for electricity generation, and cooling the breeding zone and structural components of the blanket. To that end, blanket designs, e.g. dual-coolant lead-lithium (DCLL) [1], feature a feeding inlet pipe which branches off into parallel channels via a manifold. After making a few passes to absorb heat and produce tritium, the heated LM is collected by another manifold to extract LM from the blanket toward the ancillary system through the connected outlet pipe.

Ensuring balanced distribution of flow among the multiple channels is a critical concern as overheating of structural material may occur in underfed channels [2]. Thus, it is important to characterize MHD flow through manifold components and identify factors that affect flow balance in multichannel MHD flows.

Numerical modeling has been an effective tool for probing the behavior of MHD flows in manifolds with transverse applied magnetic field. Recent numerical studies suggest control of flow distribution among multiple channels is possible as demonstrated by adjusting the geometry of a prototypic manifold which feeds three parallel channels (Fig. 1). It was shown that increasing expansion length, L_{exp} , for small values of channel length, L_{chan} , tends to balance the flow [3]. Small L_{exp} caused the side channels to be underfed. In the present work, we show that increasing L_{chan} has a balancing influence on the flow distribution. The system

is shown to behave analogously to a Resistor Network Model (RNM), which we introduce in the present work. Steady state, fully 3D MHD solutions are obtained using HIMAG [4] to study the influence of channel length on flow distribution in an electrically insulated prototypic inlet manifold.

2. Numerical Methodology

Steady solutions for laminar flow of liquid metal through an electrically insulated manifold (Fig.1) in a strong transverse magnetic field are obtained numerically. Such a flow is characterized by the following key dimensionless parameters: Hartmann number, $Ha = bB\sqrt{\sigma_f/\rho\nu}$ where B , σ_f , ρ , and ν are applied magnetic field strength, fluid electrical conductivity, density, and kinematic viscosity respectively; Reynolds number, $Re = Ub/\nu$; expansion ratio, $r_{exp}=b/d$; dimensionless duct height, a/d ; dimensionless length of the expansion region, L_{exp}/b ; dimensionless length of the multiple channels, L_{chan}/b ; and channel size parameter, $s_c=h/b$. In the present work $Ha=1465$, $Re=100$, $r_{exp}=4$, $a/d=0.8$, $L_{exp}/b=0.5$, and $s_c=0.3$ while $L_{chan}/b=[2, 10, 20, 30, 40, 50]$.

Using the Hoffman2 computer cluster at UCLA, each simulation was run in parallel on 128 nodes until steady state solutions were reached as determined by the L2 norm of the residuals reaching the order of 10^{-16} . Here, residuals are defined as the difference of flow variables at consecutive time steps.

*corresponding author's email: tyler@fusion.ucla.edu (Tyler J. Rhodes)

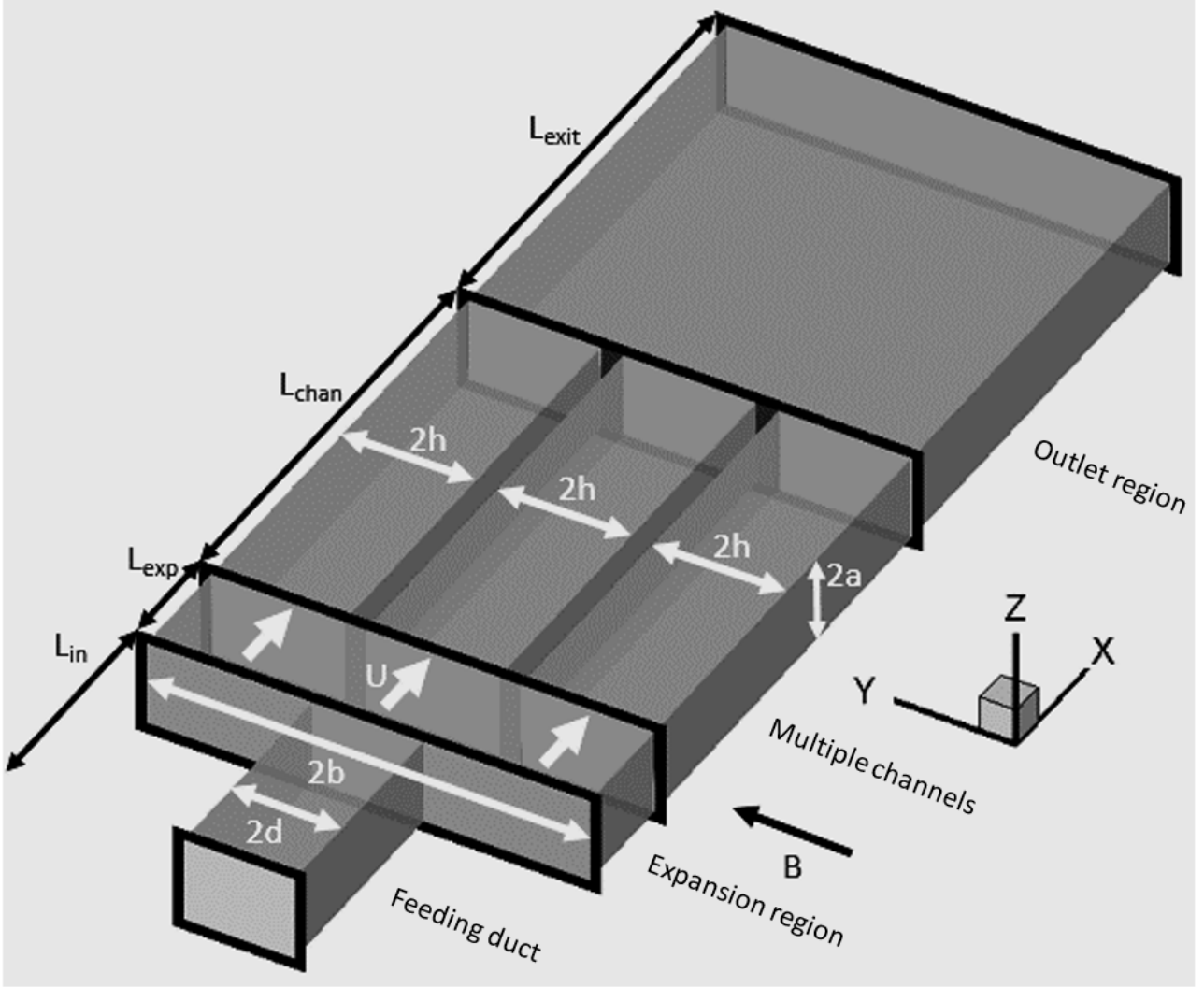


Figure 1: A prototypic manifold geometry with attached parallel channels for numerical simulation. Fully developed flow enters the feeding duct, spreads out into the expansion region, is sorted into multiple channels, and collects in the common outlet where it becomes fully developed before exiting the duct.

2.1 Governing equations

The incompressible MHD equations, shown below (1-4), include an electric potential formulation for Maxwell's equations along with the Navier-Stokes equations. It is assumed that the magnetic Reynolds number is small such that the induced magnetic field is neglected compared to the applied one:

Continuity equation for incompressible flow,

$$\nabla \cdot \mathbf{u} = 0; \quad (1)$$

Navier-Stokes equation,

$$\frac{\partial \mathbf{u}}{\partial t} + \mathbf{u} \cdot \nabla \mathbf{u} = -\frac{1}{\rho} \nabla p + \nu \nabla^2 \mathbf{u} + \frac{1}{\rho} \mathbf{J} \times \mathbf{B}; \quad (2)$$

Ohm's law,

$$\mathbf{J} = \sigma(-\nabla \varphi + \mathbf{u} \times \mathbf{B}); \quad (3)$$

Continuity equation for electrical current,

$$\nabla \cdot \mathbf{J} = 0. \quad (4)$$

Here, \mathbf{u} , \mathbf{J} , and \mathbf{B} are the velocity, electrical current density, and magnetic field vectors respectively and p

and φ are the pressure and electric potential. ν is kinematic viscosity. Taking the divergence of Eq. (3) and combining with Eq. (4), we obtain a common electrical potential formulation:

$$\nabla \cdot (\sigma \nabla \varphi) = \nabla \cdot (\sigma \mathbf{u} \times \mathbf{B}). \quad (5)$$

To consider both the liquid and the surrounding solid wall, which may have different electrical conductivity, the electrical conductivity σ is left inside the derivatives in Eq. (5).

2.2 Computational mesh

Eqs. (1, 2, 5) were solved numerically on non-uniform rectangular meshes (Fig. 2) which were previously evaluated in a mesh refinement study using the same solver and similar parameters. The mesh refinement study used three meshes: a coarse mesh (~0.5 million cells), a medium mesh (~1 million cells), and a fine mesh (~2 million cells). In the present computations, the fine mesh was used. In making each mesh, we ensured that there are at least 5 nodes inside all Hartmann layers on the walls perpendicular to the magnetic field and 12 nodes inside each side layer on the

wall parallel to the magnetic field. Also, higher mesh resolution was used in the liquid next to the back wall of the expansion region, which is perpendicular to the axial direction, where internal shear layers might be formed.

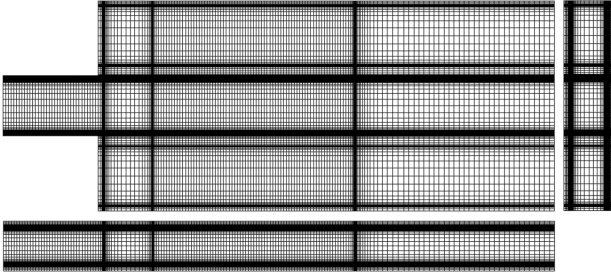


Figure 2: An example computational mesh with 2.05 million cells for a manifold geometry with 3 channels, $L_{exp}/b=0.5$, $L_{chan}/b=2$, $r_{exp}=4$, $s_c=0.3$, and $a/d=0.8$.

2.3 Initial and boundary conditions

Simulations were started with initially uniform flow conditions with a time step size $\Delta t=10^{-4}$ s. Fully developed Shercliff flow is used as the inlet boundary condition in the feeding duct. The outlet boundary condition is in the form $\frac{\partial}{\partial x} = 0$ for all variables except pressure. The pressure is set to zero at the outlet and the fully developed Shercliff pressure gradient is used at the inlet. The no slip condition is enforced at all fluid-wall interfaces. Normal components of electrical current density are set to zero at the outer domain boundary to agree with the fully developed inlet and outlet conditions.

2.4 Numerical Solver

The full MHD equations shown in section 2.1 are solved using HyPerComp/UCLA's MHD solver, HIMAG (HyPerComp Incompressible MHD solver for Arbitrary Geometries). Details regarding the formulation and validation of the HIMAG code can be found elsewhere (e.g. [4, 5]).

3. Results & discussion

In Fig. 3, the percentage of the total flowrate carried by each channel is plotted versus L_{chan} .

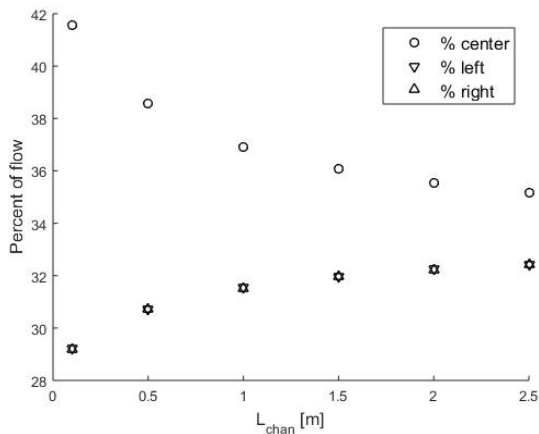


Figure 3: Percentage of the total flowrate carried by each of the three channels is plotted.

The curves for the left and right channels overlap because the flow is symmetrical for the study's parameter space. The manifold flow becomes more balanced as L_{chan} increases, tending towards perfectly balanced flow where each channel carries a third of the total flowrate. The behavior of this effect is best described via analogy to an electrical circuit segment. In this analogy, our manifold geometry is simplified as a Resistor Network Model (RNM) composed of three parallel pairs of resistors as illustrated in Fig. 4.

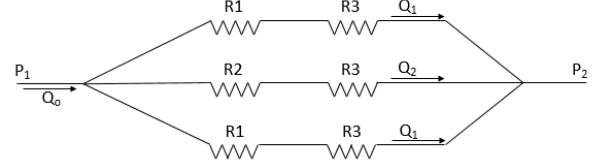


Figure 4: A Resistor Network Model of the prototypical manifold in Fig. 1.

Here, the three parallel channels of the manifold are represented by three identical resistors with variable resistance $R3$ which increases linearly with L_{chan} . The resistors labeled $R1$ and $R2$ have constant resistance and represent the 3D flow in the expansion region which feeds each of the three channels. Since L_{exp} is small ($L_{exp}/b < 1$), it is expected that $R2 < R1$. The flow distribution is then governed by the following equations:

$$Q_1(R1 + R3) = P_2 - P_1, \quad (6)$$

$$Q_2(R2 + R3) = P_2 - P_1, \quad (7)$$

$$Q_2 = \frac{(\%center)}{100} Q_o, \quad (8)$$

$$Q_1 = \frac{100 - (\%center)}{200} Q_o. \quad (9)$$

Equations (6-7) are analogous to Ohm's law such that electrical current is to flowrate Q as voltage is to pressure P . Eqs. (8-9) relate the total flowrate Q_o and channel flowrates Q_1 and Q_2 to the percentage of the total flowrate carried by the center channel ($\%center$).

Assuming that the development length of the flow in the channels is small compared to L_{chan} , we may define $R3$ as follows:

$$R3 = L_{chan}S. \quad (10)$$

Here, S is the Shercliff pressure gradient in a fully developed flow [6] per flowrate. Combining Eqs. (6-10) yields

$$(\%center) = 100 \frac{L_{chan}S + R1}{3L_{chan}S + 2R2 + R1}. \quad (11)$$

The resulting Eq. (11) matches our intuition that as L_{chan} approaches infinity, ($\%center$) approaches 33.3...%. Values for $R1$ and $R2$ cannot be determined analytically due to the complexity of the flow in the expansion region; however, we have determined values for $R1$ and $R2$ by curve fitting Eq. (11) to numerical data for ($\%center$).

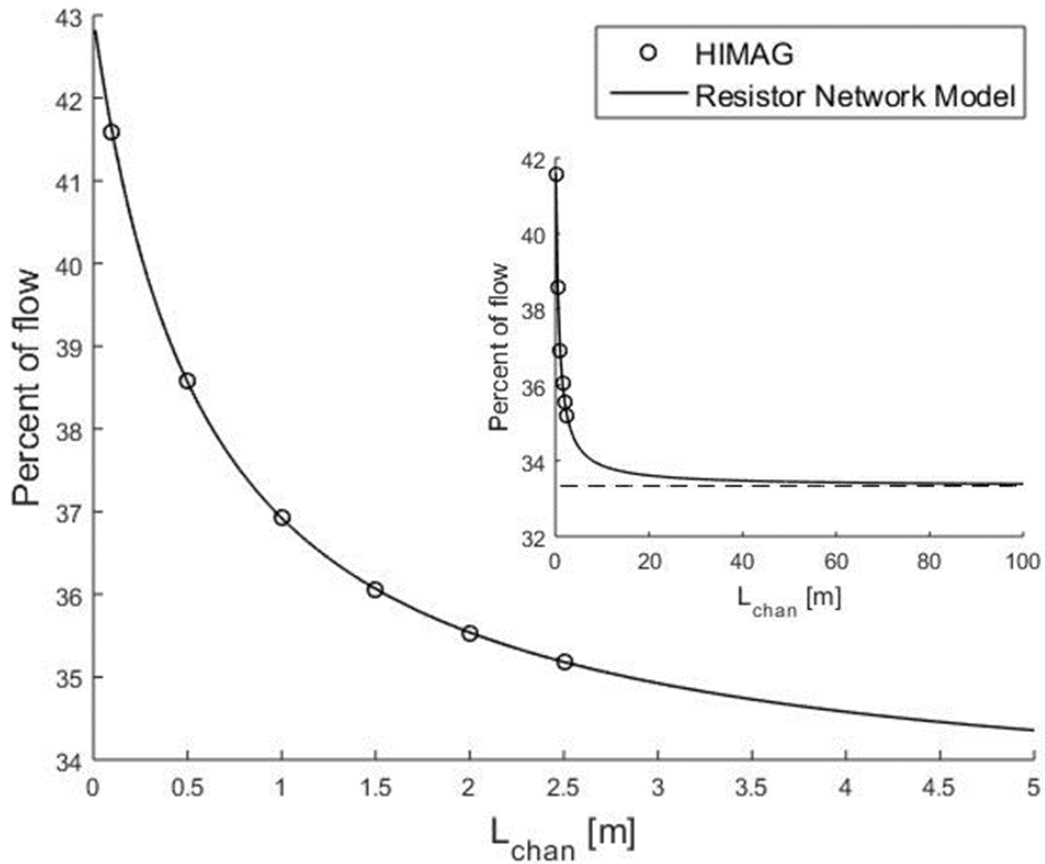


Figure 5: An RNM is fit to the numerical results for (%center). The smaller plot shows the modelled behavior of the flow distribution for much larger channel length. The flowrate carried by the center channel approaches 1/3 of the total flowrate as L_{chan} increases.

Using a minimization algorithm, we select values of R1 and R2 which minimize the Root Mean Squared Deviation (RMSD) comparing the 3D numerical results and Eq. (11). Given the pressure gradient in a fully developed flow $S=8.800 \times 10^6 \text{ Pa}\cdot\text{s}/\text{m}^4$ for the reference magnetic field and flow velocity specified in Section 2, Eq. (11) best fits the data when R1 and R2 equal $6.726 \times 10^6 \text{ Pa}\cdot\text{s}/\text{m}^3$ and $4.462 \times 10^6 \text{ Pa}\cdot\text{s}/\text{m}^3$ respectively. The resulting RNM fits the numerical data with an RMSD of 0.0067. The model is plotted along with the numerical data in Fig. 5. In addition to fitting the numerical data well, the RNM is shown to agree with the expected behavior of the manifold as L_{chan} increases past 2.5m. It is worth noting that in this case, the modelled (%center) comes within 1% of the perfectly balanced value (34.33...%) after L_{chan} exceeds 5m.

Since there are two unknowns in the RNM, R1 and R2, it is possible to fully define the RNM using only two simulations or experiments. That is, if we know (%center) for each of two values of L_{chan} , we can solve Eq. (11) for the constants R1 and R2 at a particular Ha and Re . Below, we demonstrate by calculating R1 and R2 for each possible pair of simulations we have performed.

We have six simulations with different channel lengths so the number of unique pairs of channel lengths

is $15 = \frac{1}{2} \left[\frac{6!}{(6-2)!} \right]$. Thus we can calculate 15 pairs of resistor values R1 and R2. The computed resistor values are plotted in Fig. 6 versus the sum of the two channel lengths used for each calculation.

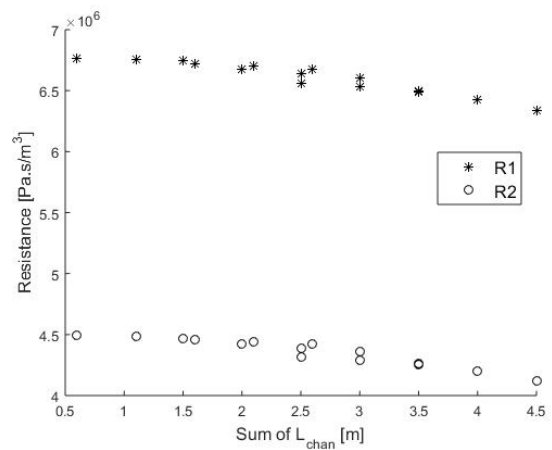


Figure 6: Resistor values are plotted against the sum of each pair of channel lengths used for the calculations.

A slight decreasing trend is observed even though the model stipulates that R1 and R2 are constants that are not dependent on L_{chan} . Still, the calculated resistances are within 5.7% and 7.7% of the best fit values of R1 and R2 respectively. To get an idea for how these errors

affect the model's applicability, we compare the RNMs using the highest and lowest calculated resistor values along with the numerical data in Fig. 7.

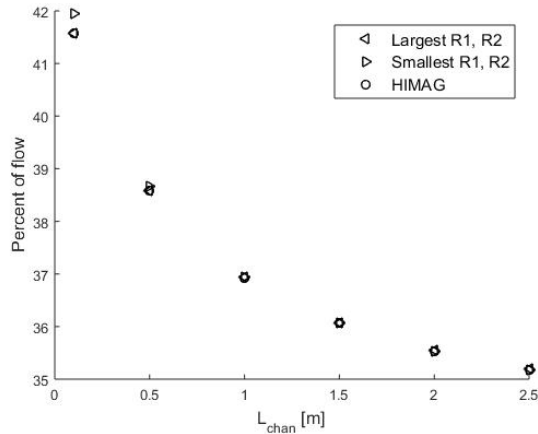


Figure 7: Two RNMs, each with the highest or lowest values of resistors R1 and R2, are compared to numerical values of the percentage of total flowrate carried by the center channel.

The maximum difference between the two models and the numerical data is 0.36% (at $L_{chan}=0.1m$) and the error is an order of magnitude smaller for $L_{chan}>1m$. Thus all of the calculated resistor pairs are suitable for predicting the flow distribution as a function of L_{chan} with acceptably small error. This is an important result because it indicates that only two simulations or experiments are required for predicting the flow distribution for the full range of L_{chan} .

4. Conclusions

We simulated MHD flow through a non-conducting manifold using HIMAG with parametric variations of L_{chan} , the length of the three parallel channels fed by the manifold.

We observed that increasing L_{chan} causes flow to become more evenly distributed among the parallel channels. Furthermore, a Resistor Network Model was introduced to model the flow distribution as a function of L_{chan} . The RNM was shown to fit the flow distribution data as well as the expected behavior of the flow distribution as L_{chan} becomes very large. In the present case, it was shown that prohibitively long channels would be required to achieve a balanced flow distribution ($L_{chan}\sim 5m$ for 34.33% of flow passing through the center channel). However, this problem may be mitigated by increasing the length (L_{exp}) between the sudden expansion and the inlets of the parallel channels [3] or by electrically coupling the channels [7].

As a design tool, the proposed RNM is useful because only two simulations or experiments are required to determine a channel length which produces a desired flow distribution given a set of flow parameters and manifold geometry. By contrast, other methods for optimizing channel length will require more than two iterations. Thus using an RNM may save blanket designers months or years of computational time and may prevent the need for many expensive experiments for optimizing blanket designs.

The model is not limited to the particular manifold configuration of three parallel channels and can easily be extended to a more complex configuration, though for other configurations the RNM would require validation. For instance, changing L_{exp} or adding a sudden contraction to the outlet is likely to only affect the values of R1 and R2 in Eq. (11). Additionally, the RNM is likely to be applicable for non-rectilinear ducts. The model can be generalized to n channels, taking the form of n parallel resistors. In that case, n data points will be required to fully define the RNM and solve for the n unknown resistor values. If the problem is symmetric as in the present work, the number of unknowns (and required data points) will be reduced to $n/2$ (rounded up).

Acknowledgements

This work was performed with support from US Department of Energy, Office of Fusion Energy Sciences, under Grant No. DE-FG02-86ER52123.

This work used computational and storage services associated with the Hoffman2 Shared Cluster provided by UCLA Institute for Digital Research and Education's Research Technology Group.

References

- [1] S. Smolentsev, Morley, M. A. Abdou, and S. Malang. Dual-coolant lead-lithium (DCLL) blanket status and R&D needs. *Fusion Eng. Des.* 100 (2015): 44-54.
- [2] S. Smolentsev, R. Moreau, L. Buhler, and C. Mistrangelo, MHD thermofluid issues of liquid-metal blankets: Phenomena and advances. *Fusion Eng. Des.* 85(7-9), (2010) 1196-1205.
- [3] S. Smolentsev, T. Rhodes, G. Pulugundla, C. Courtessole, M. Abdou, S. Malang, M. Tillack, and C. Kessel, MHD thermohydraulics analysis and supporting R&D for DCLL blanket in the FNSF. *Fusion Eng. Des.* (2017). Pages are available
- [4] S. Smolentsev, N. Morley, M. Abdou, R. Munipalli, R. Moreau, Current approaches to modeling MHD flows in the dual coolant lead lithium blanket, *Magnetohydrodynamics* 42.2-3 (2006) 225-236.
- [5] R. Munipalli, S. Shankar, M. Ni, N. Morley, Development of a 3-D Incompressible Free Surface MHD Computational Environment for Arbitrary Geometries: HIMAG, DOE SBIR phase-ii final report, (2003).
- [6] J. Shercliff, Steady motion of conducting fluids in pipes under transverse magnetic fields, *Mathematical Proceedings of the Cambridge Philosophical Society*, 49, (1953) 136-144.
- [7] C. Mistrangelo, L. Böhler, Electric flow coupling in the HCLL blanket concept, *Fusion Eng. Des.* 83 (2008) 1232-1237.